Electronic Supplementary Material (ESI) for Dalton Transactions.

Solvent-assisted structural conversion involving bimetallic complexes based on tris(oxalato)ferrate(III) unit with the green → blue → red crystals color sequence

Tadeusz M. Muzioł[1*], Natalia Tereba[1], Robert Podgajny[2], Dariusz Kędziera[1], Grzegorz Wrzeszcz[1]

[1] Faculty of Chemistry, Nicolaus Copernicus University in Toruń, Gagarina 7, 87-100 Toruń, Poland

[2] Faculty of Chemistry, Jagiellonian University, Gronostajowa 2, 30-387 Kraków, Poland

Supplementary materials

---

[*] corresponding author

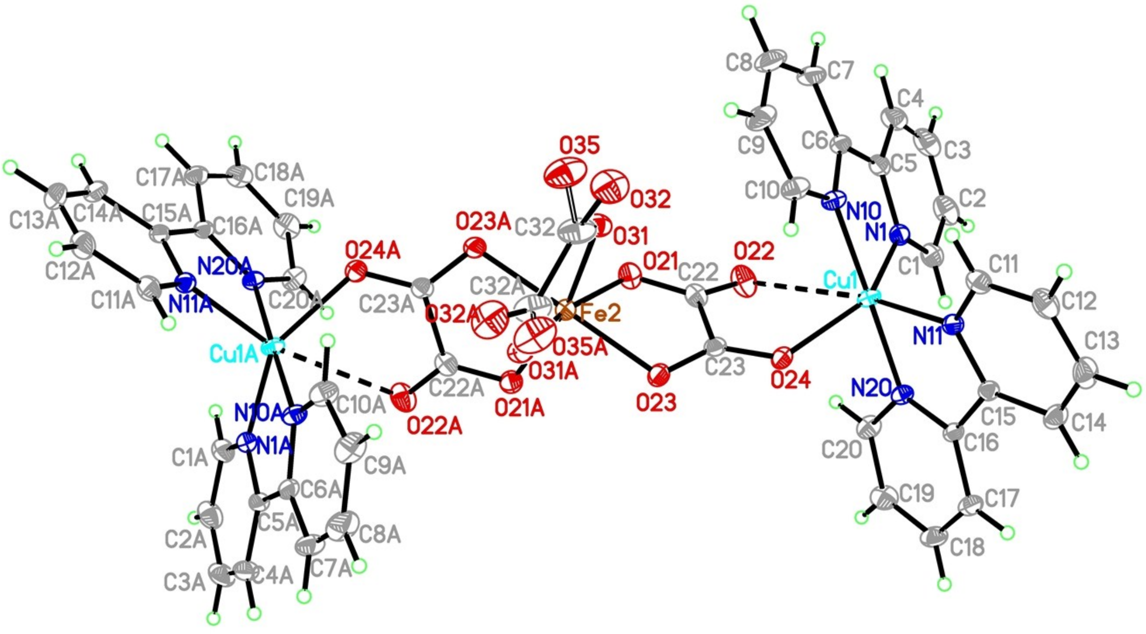

Fig. S1 The $[Cu_2(bpy)_4Fe(ox)_3]^+$ (**1**) trimer is presented and nitrate as well as water molecule are skipped. For the clarity of the picture the thermal ellipsoids are at 20% probability.

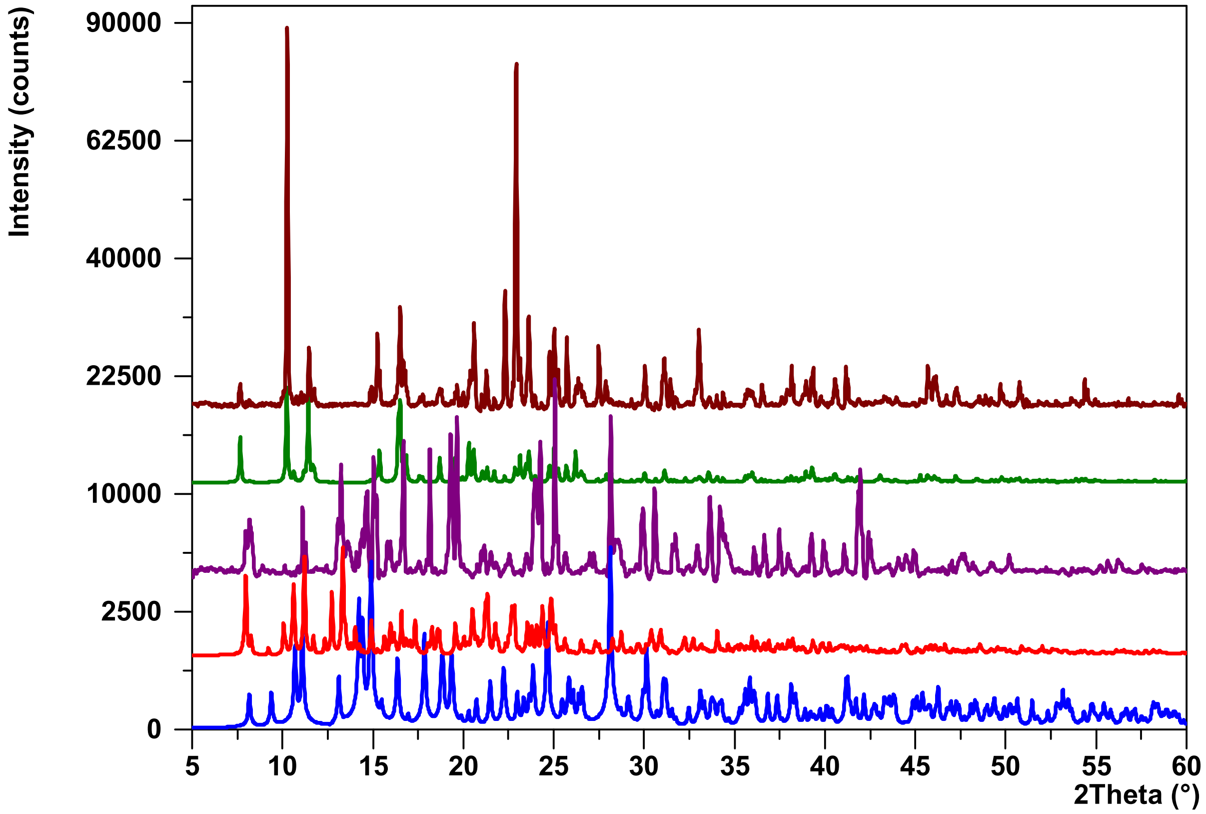

Fig. S2 Superimposed powder diffractograms of **1** (experimental, brown), **1** (calculated, green), conversion products of **1** (experimental, violet), **2a** (calculated, red), $[Cu_2(bpy)_2(ox)(H_2O)_2][Cu(bpy)(ox)](NO_3)_2$ (calculated, blue).

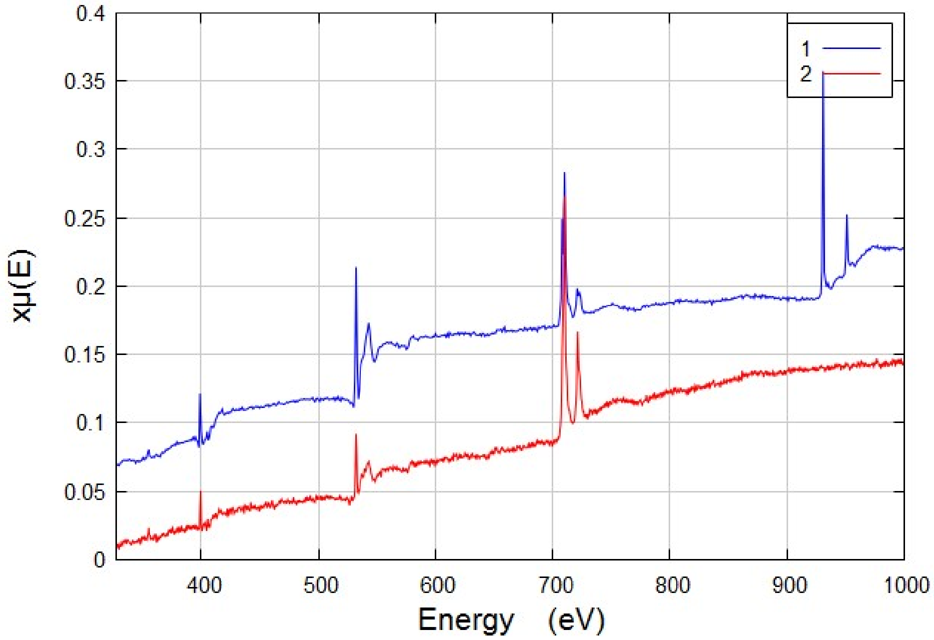

Fig. S3 XANES spectrum for **1** and **2**. The broad range spanning over K edges of N (*ca.* 400 eV) and O (*ca.* 530 eV) as well as L edges of Fe (*ca.* 710 eV) and Cu (*ca.* 930 eV). This spectrum clearly shows absence of XAS signal corresponding to copper for **2,** confirming that this product of the conversion is copperless complex.

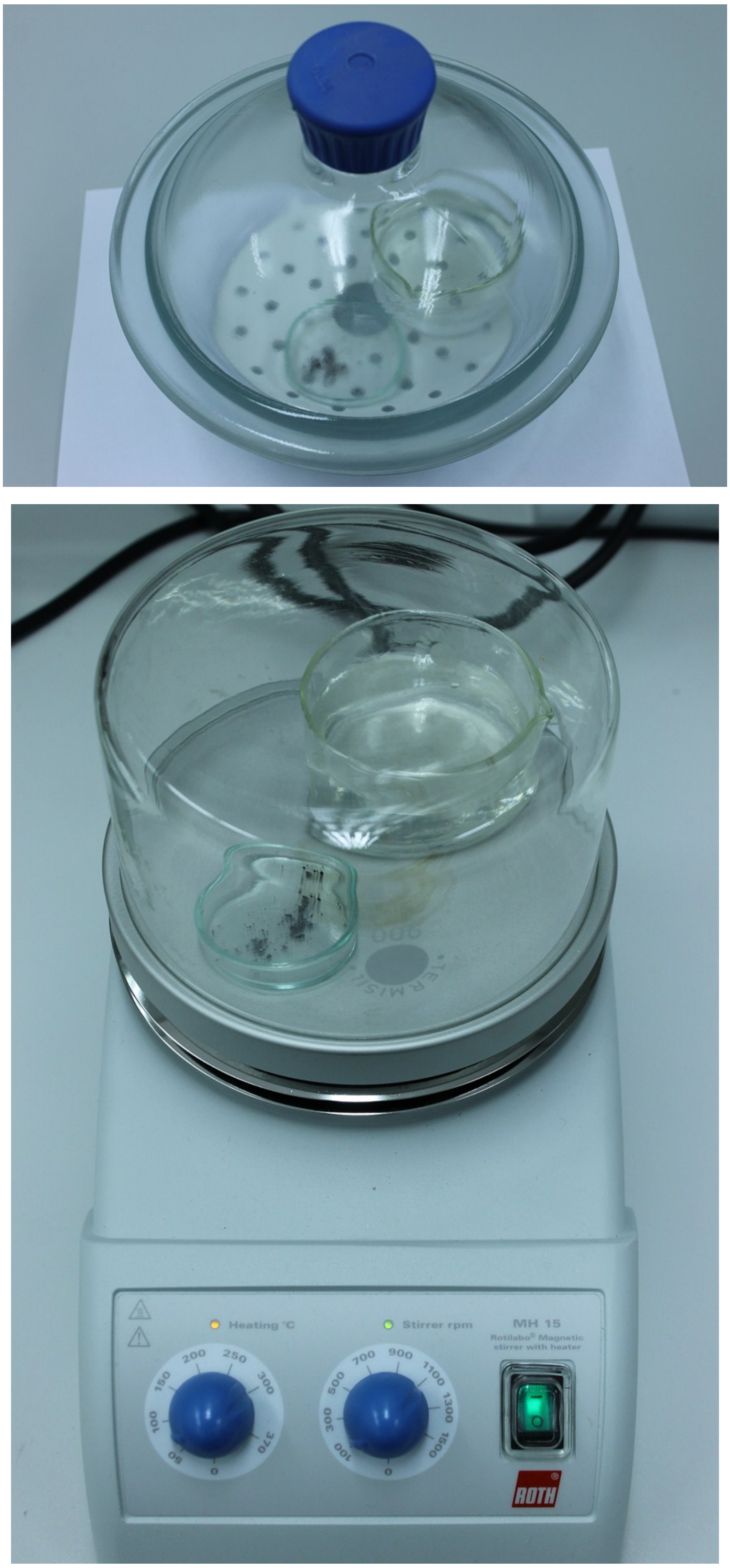

Fig. S4 Laboratory system for studying of vapors influence on the stability of trimer crystals with moderate heating to 50°C (top) and without heating (bottom). For experiments performed in the darkness these experiments were performed in vessels firmly covered with opaque material.

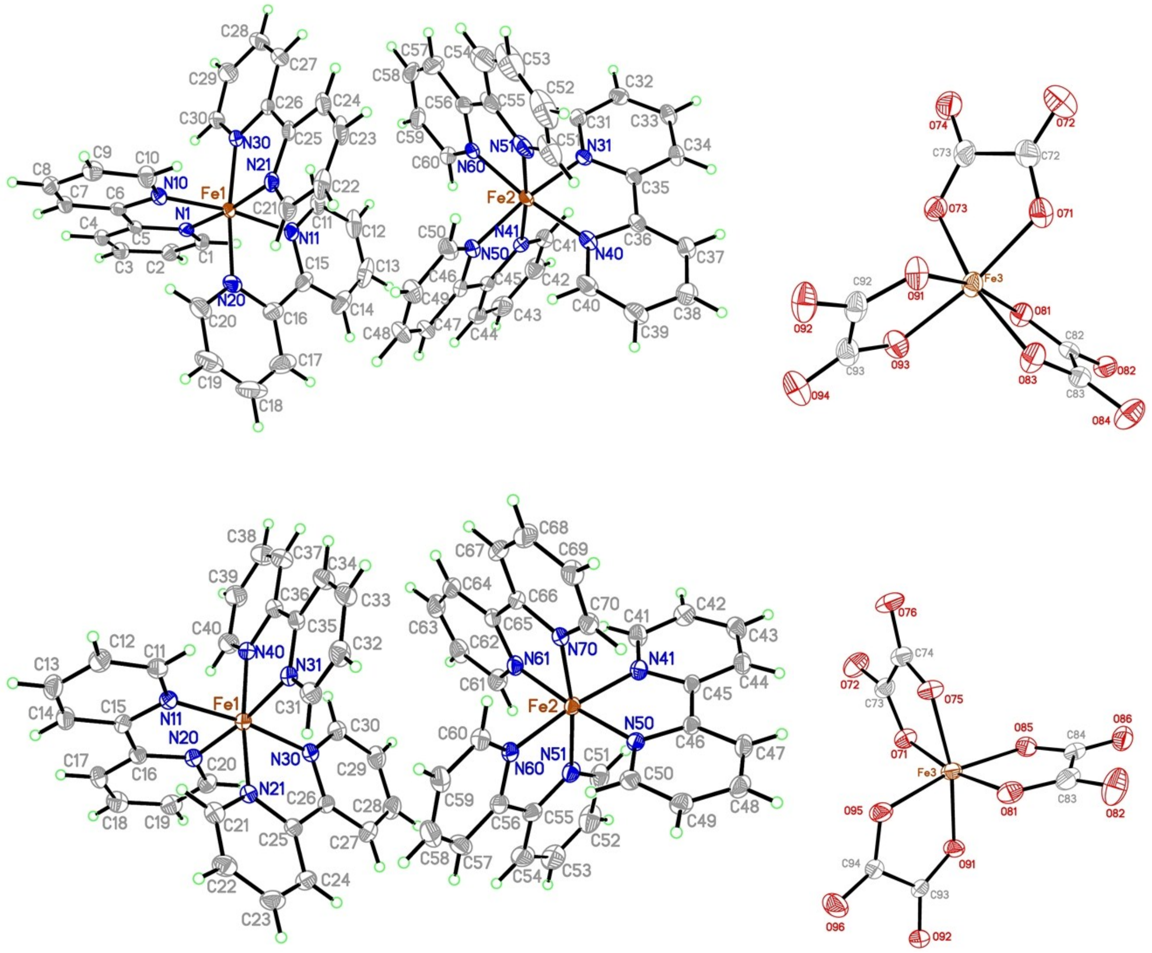

Fig. S5 The $[Fe(bpy)_3]_2[Fe(ox)_3]NO_3\cdot 10H_2O$ (**2a**) (top) and (**2**) (bottom) are presented and nitrate as well as water molecules are skipped for the clarity of the picture. The thermal ellipsoids are at 50% and 30% probability, respectively.

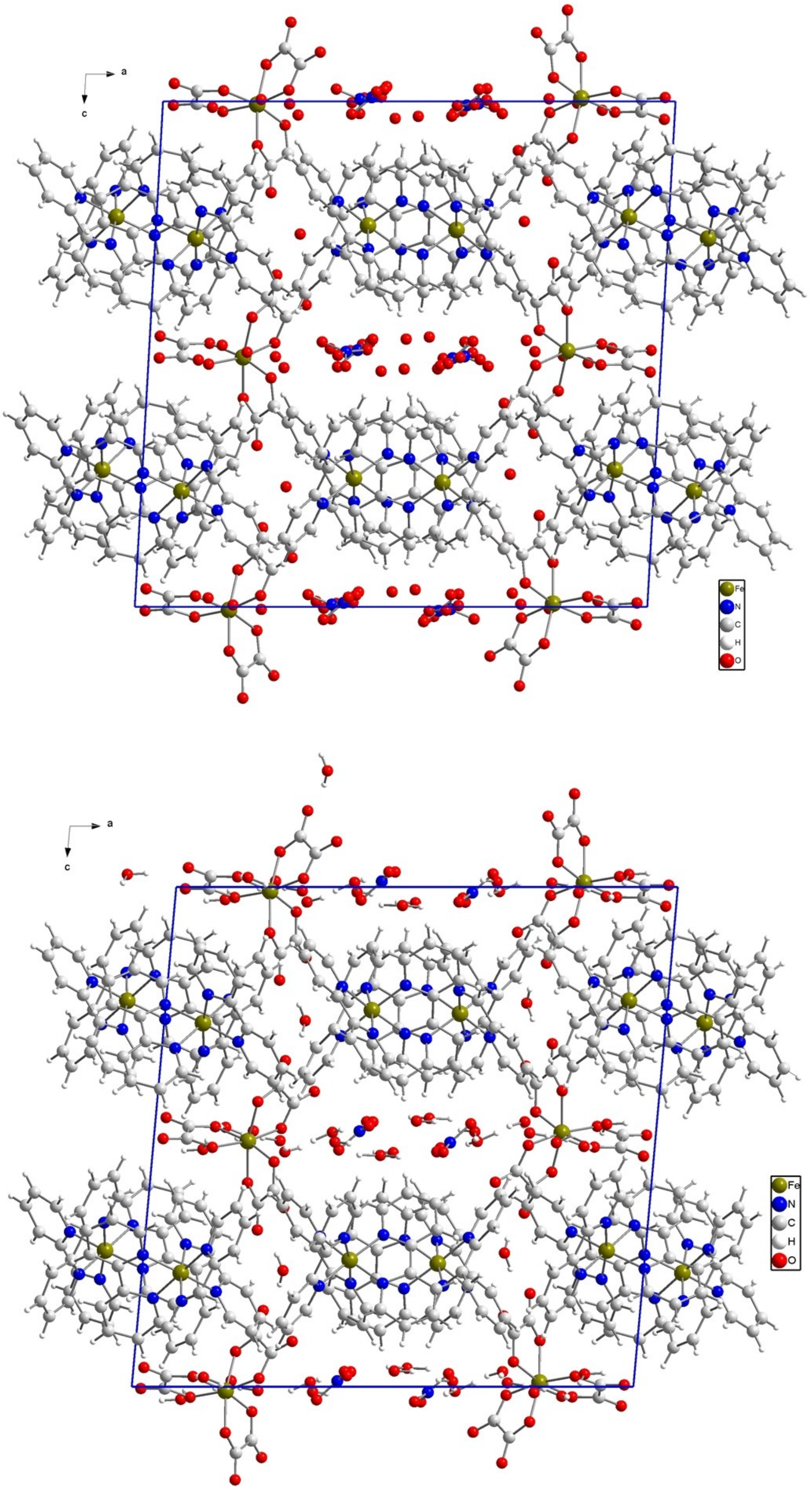

Fig. S6 Packing of (**2**) (top) and (**2a**) (bottom) along *b* axis reveals alternately arranged hydrophilic and hydrophobic *ac* sublattices.

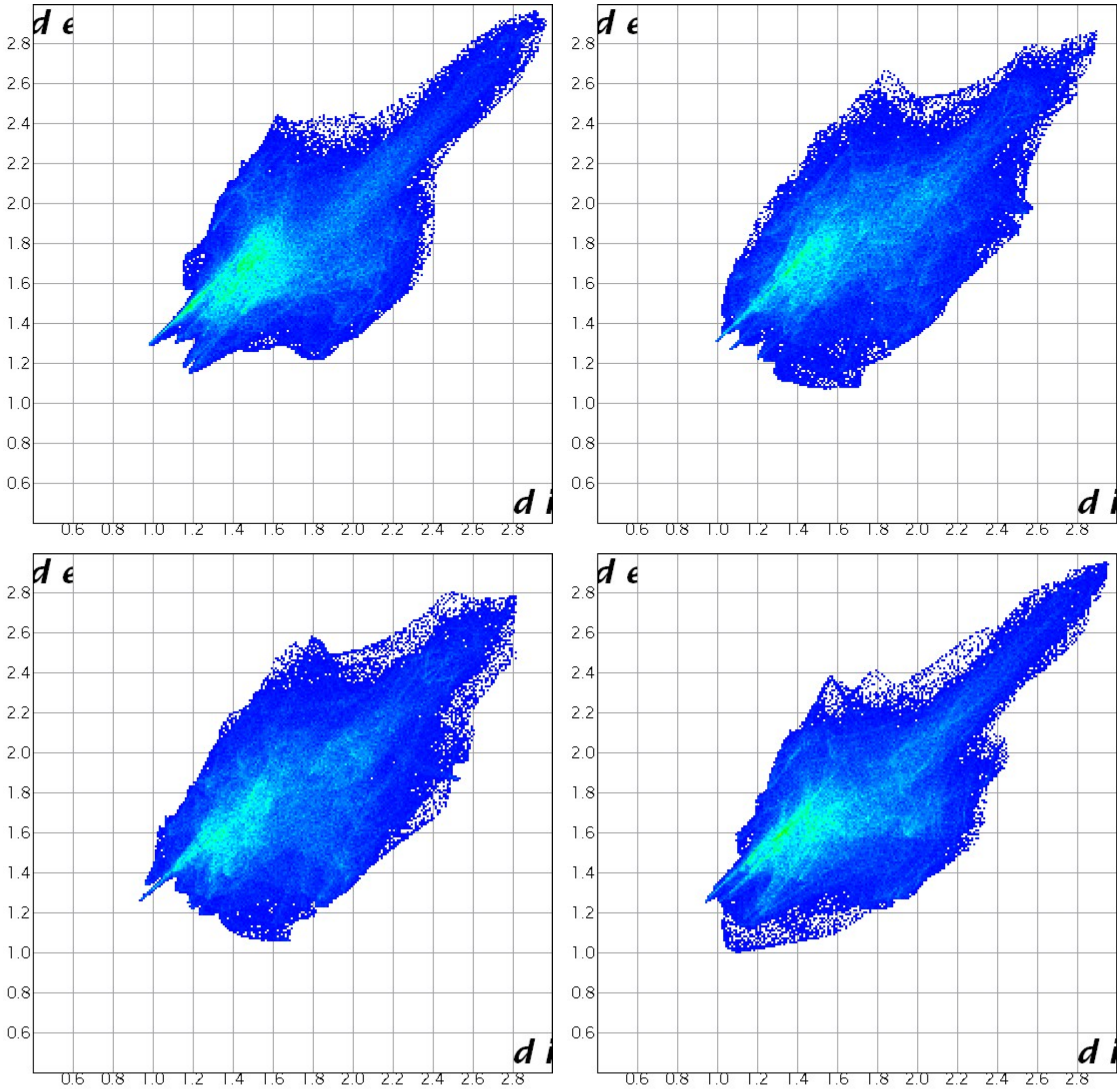

Fig. S7 Fingerprint plots of intermolecular interactions for Fe1 (left) and Fe2 (right) blocks ($[Fe(bpy)_3]^{2+}$) prepared in Crystal Explorer [1] clearly shows that both iron blocks form different interaction patterns. In the upper row two blocks for (**2**) are given, whereas in the lower for (**2a**).

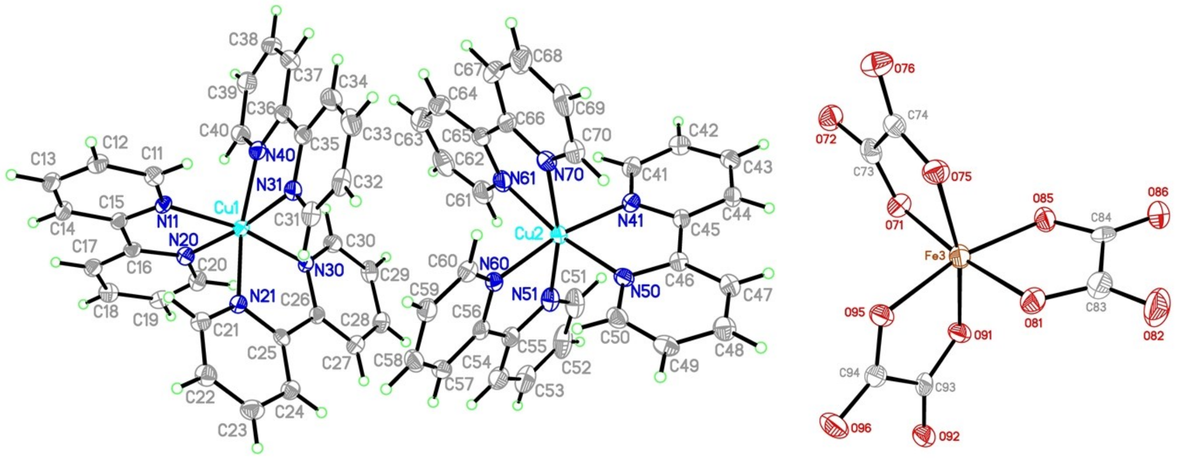

Fig. S8 Complex blocks of $[Cu(bpy)_3]_2[Fe(ox)_3]NO_3 \cdot 10H_2O$ (**3**) are presented (copper(II) units on the left and in the middle, and iron(III) on the right), whereas nitrate and water molecule are skipped. For the clarity of the picture the thermal ellipsoids are at 50% probability.

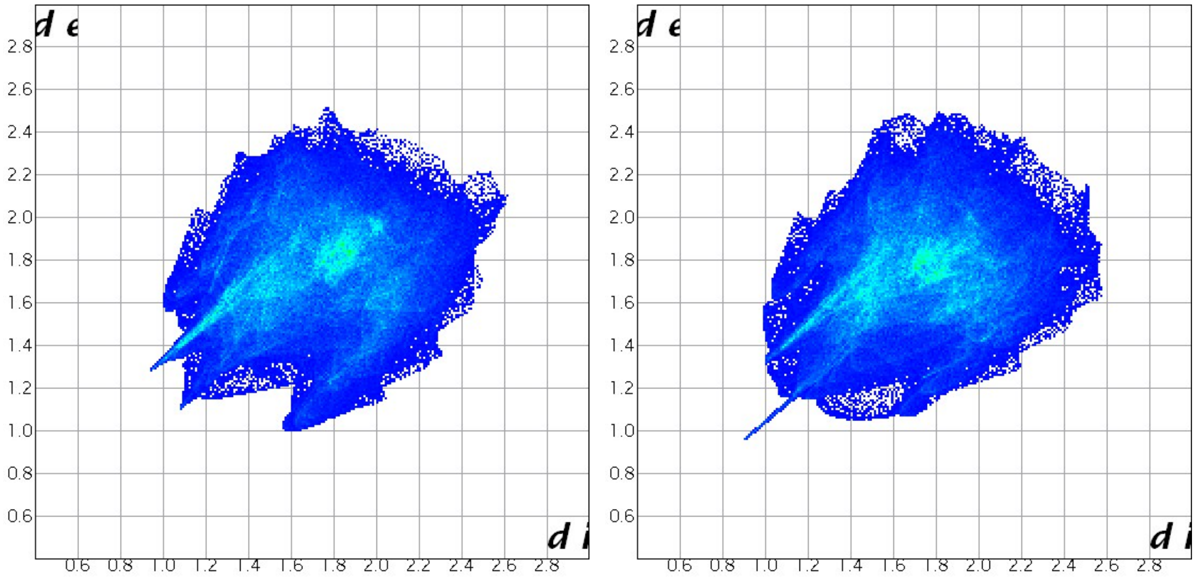

Fig. S9 Fingerprint plots of intermolecular interactions for Cu1 (left) and Cu2 (right) blocks ($[Cu(bpy)_3]^{2+}$) in (**3**) prepared in Crystal Explorer clearly shows that both copper blocks form different interaction patterns.

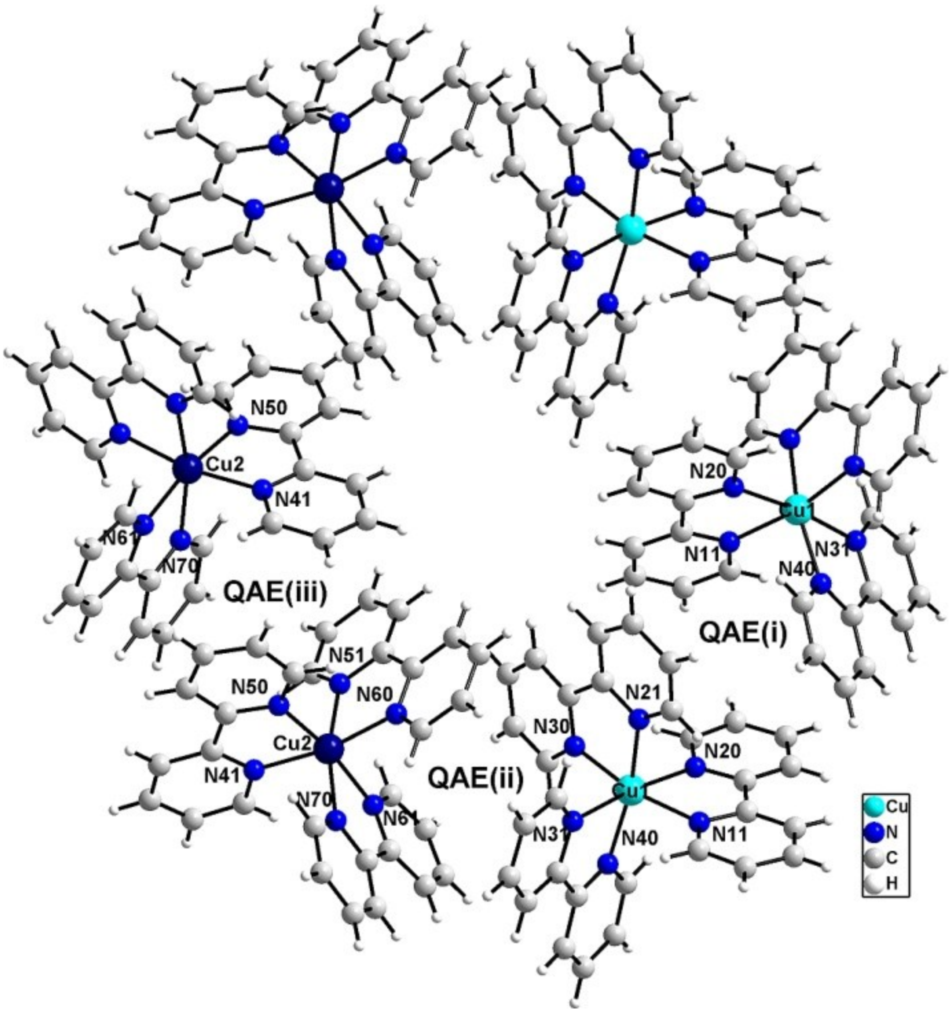

Fig. S10 Honeycomb of $[Cu(bpy)_3]^{2+}$ units in $[Cu(bpy)_3]_2[Fe(ox)_3]NO_3{\cdot}10H_2O$ **3** with marked QAE contacts forming hydrophobic domain and characterized in Table S3.

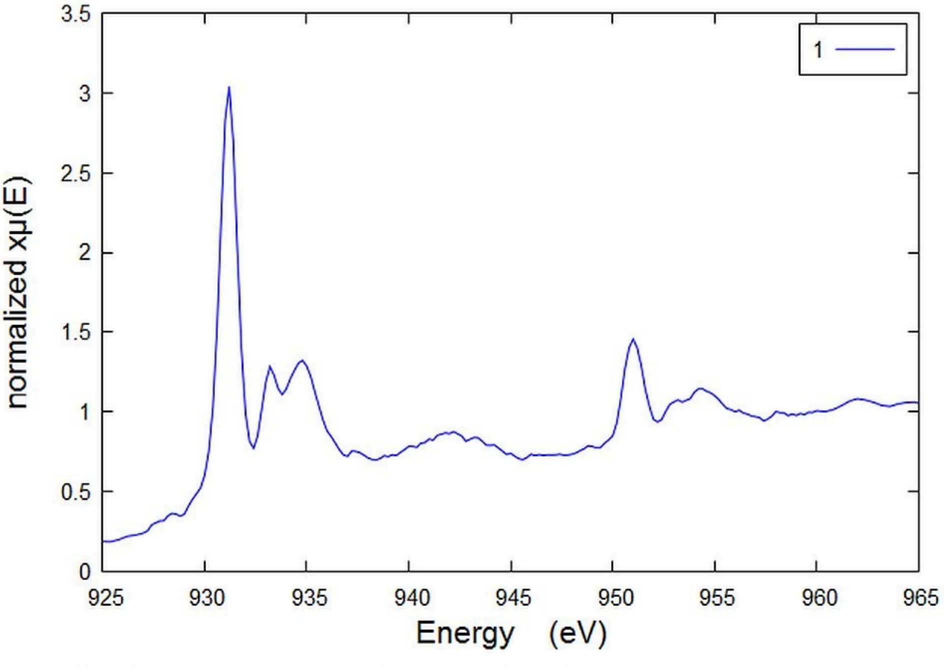

Fig. S11 Normalized XANES spectra of Cu (L-edge) for **1**.

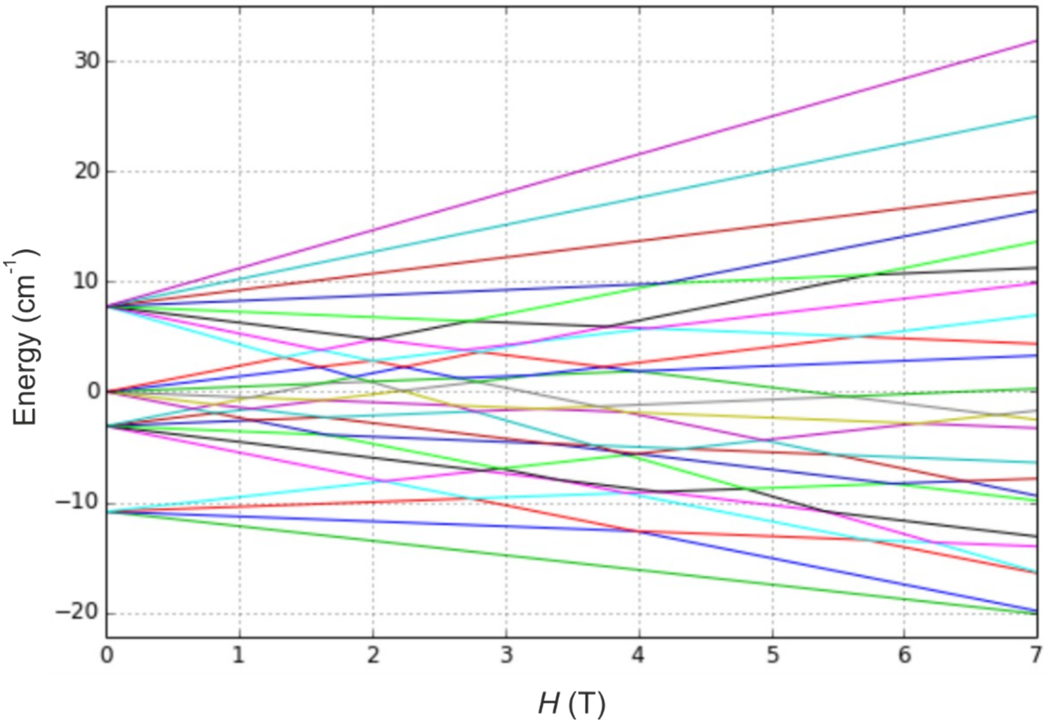

Fig. S12 The energy diagram of spin levels simulated for the symmetrical (S=$^1/_2$)-(S=$^5/_2$)-(S=$^1/_2$) system with antiferromagnetic near-neighbor exchange interactions, with $J_{\text{Cu-Fe}} = -3.1$ cm^{-1}, $g_{\text{Cu}} = 2.34$ and $g_{\text{Fe}} = 2.01$.

a

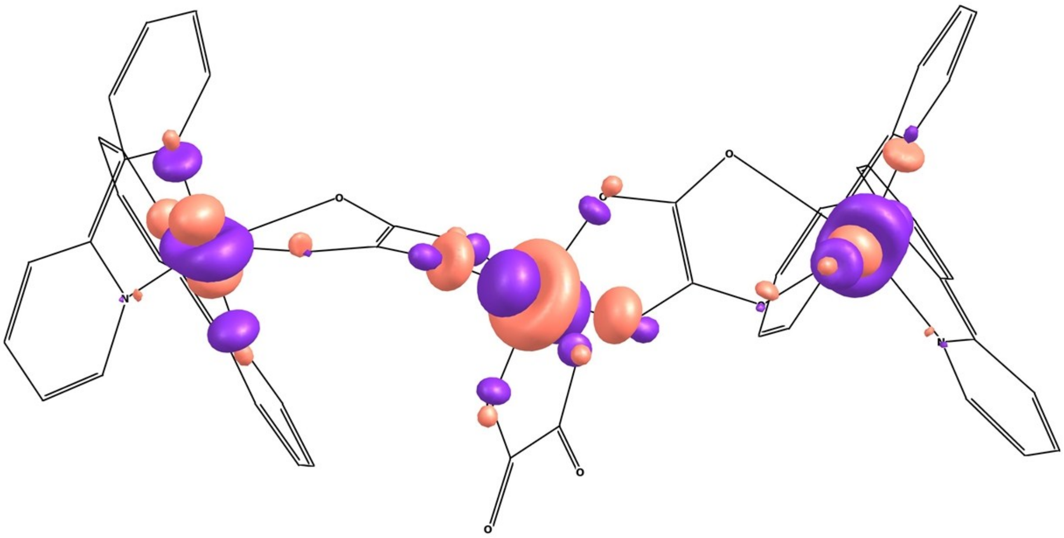

b

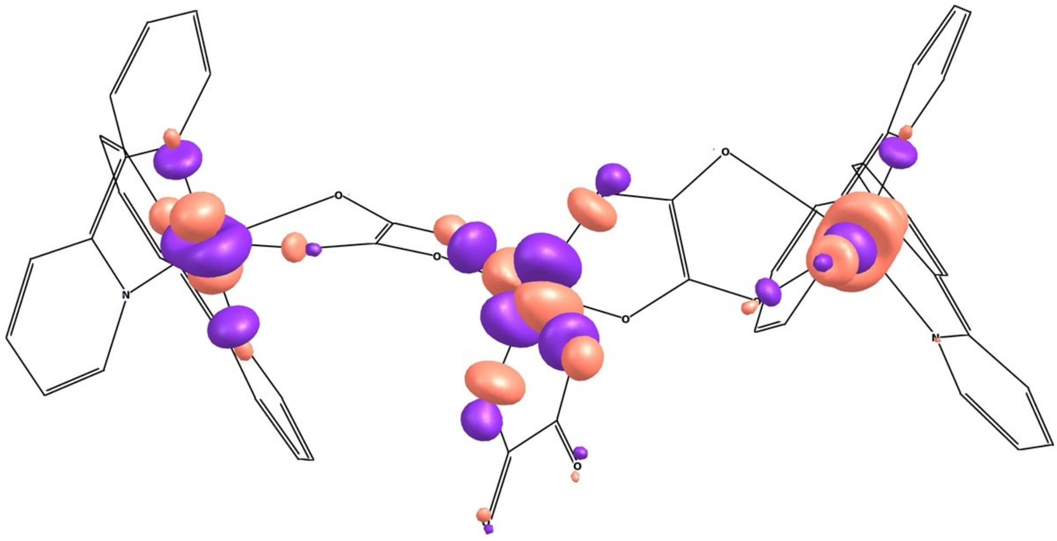

c

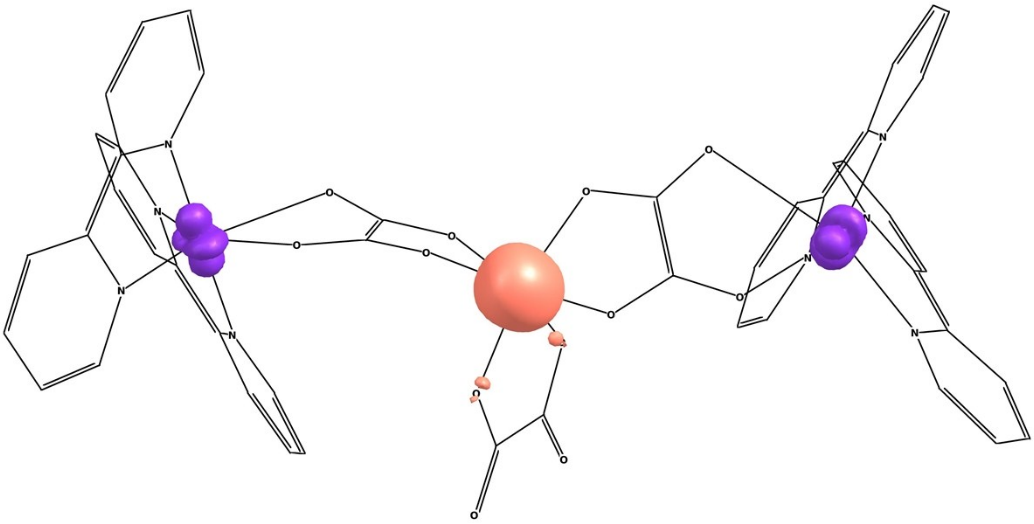

d.

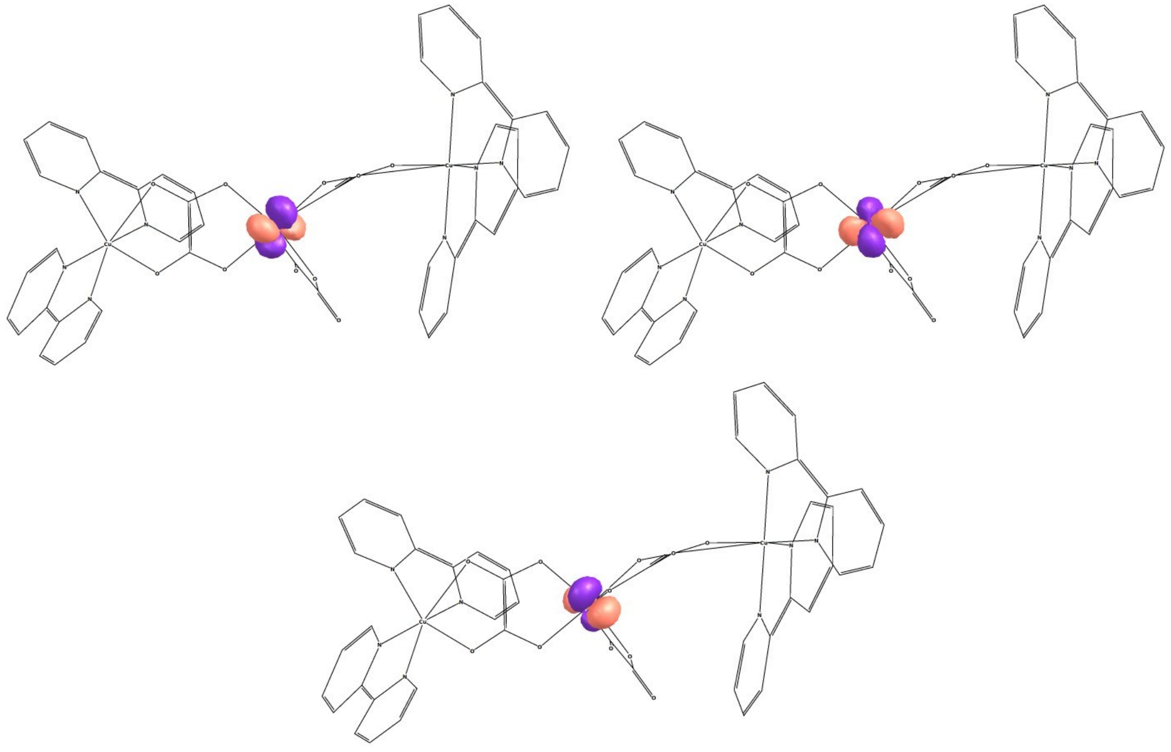

Fig. S13 The magnetic orbitals (a and b) and spin density (c) obtained from the broken-symmetry DFT calculation (broken symmetry approach, B3LYP/6-311+G* with $S_{\alpha\beta}$ values being 0.048 and 0.006 for a and b, respectively. We present also SOMO orbitals located at iron(III) and corresponding to d_{xz}, d_{yz} and d_{xy} orbitals (d). Positive and negative values are represented by red and violet surfaces, respectively.

Table S1 Crystal data and structure refinement for **1**, **2**, **2a** and **3**

Identification code	**1**	**2**	**2a**	**3**
Empirical formula	$C_{46}H_{34}Cu_2FeN_9O_{16}$	$C_{66}H_{68}Fe_3N_{13}O_{25}$	$C_{66}H_{68}Fe_3N_{13}O_{25}$	$C_{66}H_{68}Cu_2FeN_{13}O_{25}$
Formula weight	1151.75	1610.88	1610.88	1626.26
Temperature [K]	293(2)	293(2)	100(2)	100(2)
Wavelength [Å]	0.71073	0.71073	0.82657	0.7999
Crystal system, space group	Monoclinic, C2/c (no 15)	Monoclinic, $P2_1/c$ (no 14)	Monoclinic, $P2_1/c$ (no 14)	Monoclinic, $P2_1/c$ (no 14)
Unit cell dimensions [Å] and [°]	a = 16.5783(6) b = 17.2734(5) β = 111.045(4) c = 16.9386(6)	a = 22.8905(14) b = 13.7526(10) β = 93.211(6) c = 22.5276(16)	a = 22.4119(4) b = 13.8413(2) β = 95.0901(17) c = 22.4102(6)	a = 22.7927(6) b = 13.8928(4) β = 95.874(2) c = 22.2881(6)
Volume [Å^3]	4527.1(3)	7080.6(8)	6924.4(2)	7020.6(3)
Z, Calculated density [Mg·m^{-3}]	4, 1.690	4, 1.511	4, 1.545	4, 1.539
Absorption coefficient [mm^{-1}]	1.334	0.697	1.012	1.174
F(000)	2340	3332	3332	3356
Crystal size [mm]	0.310x0.180x0.150	0.510x0.350x0.090	0.500x0.100x0.100	0.300x0.070x0.060
Theta range for data collection [°]	2.450 to 26.363	2.339 to 26.372	2.857 to 31.105	2.756 to 29.996
Limiting indices	-16<=h<=20 -20<=k<=21 -19<=l<=21	-28<=h<=24 -17<=k<=8 -28<=l<=27	-28<=h<=28, -17<=k<=17, -22<=l<=22	-28<=h<=28 -17<=k<=17 -13<=l<=13
Reflections collected/unique	14570 / 4613 [R(int) = 0.0204]	33342 / 14464 [R(int) = 0.0479]	92549 / 12941 [R(int) = 0.0471]	62091 / 9257 [R(int) = 0.0780]
Completeness [%] to theta [°]	25.242° 99.7 %	25.242° 99.9 %	29.732° 92.6%	28.681° 99.0%
Max. and min. transmission	0.825 and 0.683	0.940 and 0.718	0.906 and 0.632	0.933 and 0.720
Data/restraints/parameters	4613 / 1 / 366	14464 / 33 / 1018	12941 / 17 / 1033	9257 / 30 / 1024
Goodness-of-fit on F^2	0.664	1.042	1.048	1.053
Final R Indices [I>2sigma(I)]	R1^a = 0.0271, wR2^b = 0.0821	R1^a = 0.0573, wR2^b = 0.1430	R1^a = 0.0460, wR2^b = 0.1318	R1^a = 0.0378, wR2^b = 0.0879
R indices (all data)	R1^a = 0.0358, wR2^b = 0.0885	R1^a = 0.0964, wR2^b = 0.1730	R1^a = 0.0485, wR2^b = 0.1341	R1^a = 0.0530, wR2^b = 0.0947
Largest diff. peak and hole [eÅ^{-3}]	0.321 and -0.405	0.721 and -0.493	0.850 and -0.627	0.384 and -0.412

[a] $R1 = \Sigma||F_0| - |F_C||/\Sigma|F_0|$ [b] $wR2 = [\Sigma w(F_0^2 - F_C^2)^2/\Sigma(w(F_0^2)^2)]^{1/2}$

Table S2 Selected bond length and angles for (**1**). Distances and angles formed by semi-coordinated O22 atom are marked in *italic*.

Bond lengths [Å]		Bond angles [°]			
Cu1-N10	1.9695(16)	N10-Cu1-N20	178.88(7)	O31^{i} -Fe2-O31	82.11(9)
Cu1-N20	1.9815(15)	N10-Cu1-N1	81.41(7)	O31^{i} -Fe2-O21	166.81(7)
Cu1-N1	2.0466(16)	N20-Cu1-N1	99.68(7)	O31-Fe2-O21	93.27(7)
Cu1-N11	2.1137(16)	N10-Cu1-N11	99.57(6)	O31^{i} -Fe2-O21^{i}	93.27(7)
Cu1-O24	2.1097(14)	N20-Cu1-N11	80.17(6)	O31-Fe2-O21^{i}	166.81(7)
Cu1-O22	*2.6679(18)*	N1-Cu1-N11	118.15(6)	O21-Fe2-O21^{i}	93.78(9)
Fe2-O31^{i}	1.9750(14)	N10-Cu1-O24	92.98(7)	O31^{i} -Fe2-O23^{i}	95.09(7)
Fe2-O31	1.9750(14)	N20-Cu1-O24	85.96(6)	O31-Fe2-O23^{i}	88.05(6)
Fe2-O21	2.0182(15)	N1-Cu1-O24	148.24(6)	O21-Fe2-O23^{i}	97.09(6)
Fe2-O21^{i}	2.0182(15)	N11-Cu1-O24	93.60(6)	O21^{i} -Fe2-O23^{i}	80.03(6)
Fe2-O23^{i}	2.0383(14)	*N10-Cu1-O22*	*77.81(6)*	O31^{i} -Fe2-O23	88.05(6)
Fe2-O23	2.0383(14)	*N20-Cu1-O22*	*102.11(6)*	O31-Fe2-O23	95.09(7)
		N1-Cu1-O22	*78.63(6)*	O21-Fe2-O23	80.04(6)
		N11-Cu1-O22	*162.71(6)*	O21^{i} -Fe2-O23	97.09(6)
		O24-Cu1-O22	*69.64(6)*	O23^{i} -Fe2-O23	175.84(9)

[i] -x+1,y,-z-1/2

Table S3 Interactions between aryl systems involved into QAE

Compound	**M-M distance**	**Distance bpy(I)/bpy(II')**	**Distance bpy(II)/bpy(I')**	**∠bpy(I)/bpy(II')**	**∠bpy(II)/bpy(I')**	**∠N-M-N**	**Angles between pirydyl rings**	**∠(N/O$_{\mathbf{distal}}$-Cu…Cu**
Trimer (**1**)	6.115	4.500	4.500	26.19	26.19	62.68	34.97, 34.97, 49.94, 61.29	151.03, 151.03
(**2**) QAE^{i} (Fe1-Fe1)	7.933	5.429	5.092	53.88	53.07	88.63	53.7, 47.9, 61.1, 61.6	142.10, 143.97
(**2**) QAE^{ii} (Fe1-Fe 2)	7.783	4.976	5.283	55.09	50.94	88.33	48.1, 47.4, 56.6, 64.4	139.29, 142.36
(**2**) QAE^{iii} (Fe2-Fe2)	7.792	4.733	5.914	54.87	36.35	88.36	56.3, 54.2, 59.0, 76.0	140.23, 142.46
(**2a**) QAE^{i} (Fe1-Fe1)	7.773	4.807	5.940	55.47	36.95	87.93	55.9, 38.6, 54.2, 79.1	141.15, 141.82
(**2a**) QAE^{ii} (Fe1-Fe2)	7.625	4.898	5.144	53.53	49.06	88.11	55.0, 45.4, 65.6, 56.7	139.53, 141.38
(**2a**) QAE^{iii} (Fe2-Fe2)	7.967	5.482	5.075	55.48	54.80	89.28	54.3, 50.4, 61.7, 60.4	141.90, 144.67
(**3**) QAE^{i} (Cu1Cu1)	8.097	4.969	5.646	55.46	44.02	88.29	55.48, 50.18, 62.55, 66.08	142.52, 154.15
(**3**) QAE^{ii} (Cu1Cu2)	7.674	4.478	4.851	55.36	46.68	85.81	43.39, 55.56, 61.93, 58.04	144.45, 144.33
(**3**) QAE^{iii} (Cu2Cu2)	7.791	4.543	5.828	50.53	40.96	85.86	50.48, 45.66, 58.10, 77.65	140.62, 143.22

(**1**) bpy(I) = bpy(N1), bpy(II') = bpy(N11'), bpy(II) = bpy(N11), bpy(I') = bpy(N1')
(**2**) ^{i} bpy(I) = bpy(N11), bpy(II') = bpy(N31'), bpy(II) = bpy(N21), bpy(I') = bpy(N11')
(**2**) ^{ii} bpy(I) = bpy(N21), bpy(II') = bpy(N51'), bpy(II) = bpy(N31), bpy(I') = bpy(N61')
(**2**) ^{iii} bpy(I) = bpy(N41), bpy(II') = bpy(N61'), bpy(II) = bpy(N51), bpy(I') = bpy(N41')
(**2a**) ^{i} bpy(I) = bpy(N1), bpy(II') = bpy(N21'), bpy(II) = bpy(N11), bpy(I') = bpy(N1')
(**2a**) ^{ii} bpy(I) = bpy(N11), bpy(II') = bpy(N41'), bpy(II) = bpy(N21), bpy(I') = bpy(N51')
(**2a**) ^{iii} bpy(I) = bpy(N31), bpy(II') = bpy(N51'), bpy(II) = bpy(N41), bpy(I') = bpy(N31')
(**3**) ^{i} bpy(I) = bpy(N11), bpy(II') = bpy(N31'), bpy(II) = bpy(N21), bpy(I') = bpy(N11')
(**3**) ^{ii} bpy(I) = bpy(N21), bpy(II') = bpy(N51'), bpy(II) = bpy(N31), bpy(I') = bpy(N61')
(**3**) ^{iii} bpy(I) = bpy(N41), bpy(II') = bpy(N61'), bpy(II) = bpy(N51), bpy(I') = bpy(N41')

Table S4 Selected bond lengths and angles for $[Fe(bpy)_3]_2[Fe(ox)_3]NO_3 \cdot 10H_2O$ (**2**). Data set collected at 293 K

Bond lengths [Å]		Bond angles [°]			
Fe1-N20	1.970(3)	N20-Fe1-N31	173.50(13)	N70-Fe2-N51	171.45(13)
Fe1-N31	1.971(3)	N20-Fe1-N21	90.54(13)	N41-Fe2-N51	94.78(14)
Fe1-N21	1.975(3)	N31-Fe1-N21	93.62(13)	N50-Fe2-N51	92.14(12)
Fe1-N11	1.975(3)	N20-Fe1-N11	81.59(13)	N60-Fe2-N61	91.11(12)
Fe1-N40	1.977(3)	N31-Fe1-N11	93.22(13)	N70-Fe2-N61	81.30(13)
Fe1-N30	1.981(3)	N21-Fe1-N11	92.69(12)	N41-Fe2-N61	95.36(13)
Fe2-N60	1.971(3)	N20-Fe1-N40	94.92(13)	N50-Fe2-N61	174.71(13)
Fe2-N70	1.972(3)	N31-Fe1-N40	81.28(14)	N51-Fe2-N61	92.49(13)
Fe2-N41	1.974(3)	N21-Fe1-N40	173.34(13)	O81-Fe3-O75	92.17(12)
Fe2-N50	1.978(3)	N11-Fe1-N40	91.88(13)	O81-Fe3-O91	96.42(12)
Fe2-N51	1.979(3)	N20-Fe1-N30	92.98(13)	O75-Fe3-O91	168.25(12)
Fe2-N61	1.982(3)	N31-Fe1-N30	92.58(13)	O81-Fe3-O85	80.50(13)
Fe3-O81	1.996(3)	N21-Fe1-N30	81.55(13)	O75-Fe3-O85	96.65(12)
Fe3-O75	1.999(3)	N11-Fe1-N30	172.08(13)	O91-Fe3-O85	92.67(11)
Fe3-O91	2.002(3)	N40-Fe1-N30	94.34(13)	O81-Fe3-O71	169.82(12)
Fe3-O85	2.005(3)	N60-Fe2-N70	92.62(12)	O75-Fe3-O71	80.57(12)
Fe3-O71	2.007(3)	N60-Fe2-N41	172.72(13)	O91-Fe3-O71	91.81(12)
Fe3-O95	2.011(3)	N70-Fe2-N41	91.66(13)	O85-Fe3-O71	93.17(12)
		N60-Fe2-N50	92.11(12)	O81-Fe3-O95	90.67(13)
		N70-Fe2-N50	94.35(12)	O75-Fe3-O95	91.15(12)
		N41-Fe2-N50	81.69(12)	O91-Fe3-O95	80.78(11)
		N60-Fe2-N51	81.57(14)	O85-Fe3-O95	168.40(12)
				O71-Fe3-O95	96.58(13)

Table S5 Selected bond lengths and angles for $[Fe(bpy)_3]_2[Fe(ox)_3]NO_3 \cdot 10H_2O$ (**2**a). Data set collected at 100 K

Bond lengths [Å]		Bond angles [°]			
Fe1-N30	1.971(2)	N30-Fe1-N11	92.96(8)	N50-Fe2-N51	94.92(9)
Fe1-N11	1.9706(19)	N30-Fe1-N10	92.44(8)	N31-Fe2-N51	90.87(8)
Fe1-N10	1.9715(19)	N11-Fe1-N10	171.91(8)	N41-Fe2-N51	173.83(9)
Fe1-N21	1.974(2)	N30-Fe1-N21	81.63(9)	N60-Fe2-N40	173.46(8)
Fe1-N1	1.9769(19)	N11-Fe1-N21	91.37(8)	N50-Fe2-N40	93.03(8)
Fe1-N20	1.980(2)	N10-Fe1-N21	95.37(8)	N31-Fe2-N40	81.75(8)
Fe2-N60	1.968(2)	N30-Fe1-N1	93.53(8)	N41-Fe2-N40	90.91(8)
Fe2-N50	1.967(2)	N11-Fe1-N1	91.82(8)	N51-Fe2-N40	94.61(10)
Fe2-N31	1.9702(19)	N10-Fe1-N1	81.84(8)	O91-Fe3-O73	97.51(8)
Fe2-N41	1.970(2)	N21-Fe1-N1	174.33(8)	O91-Fe3-O81	167.28(7)
Fe2-N51	1.975(2)	N30-Fe1-N20	172.34(8)	O73-Fe3-O81	93.74(7)
Fe2-N40	1.979(2)	N11-Fe1-N20	81.65(9)	O91-Fe3-O93	80.77(7)
Fe3-O91	2.0028(18)	N10-Fe1-N20	93.51(9)	O73-Fe3-O93	94.57(7)
Fe3-O73	2.0022(17)	N21-Fe1-N20	93.01(9)	O81-Fe3-O93	92.46(7)
Fe3-O81	2.0129(18)	N1-Fe1-N20	92.09(8)	O91-Fe3-O71	92.72(8)
Fe3-O93	2.0114(18)	N60-Fe2-N50	92.75(8)	O73-Fe3-O71	80.46(7)
Fe3-O71	2.0160(18)	N60-Fe2-N31	92.76(8)	O81-Fe3-O71	95.00(7)
Fe3-O83	2.0289(18)	N50-Fe2-N31	172.51(8)	O93-Fe3-O71	171.28(8)
		N60-Fe2-N41	92.92(9)	O91-Fe3-O83	89.52(8)
		N50-Fe2-N41	82.01(9)	O73-Fe3-O83	167.62(8)
		N31-Fe2-N41	92.66(8)	O81-Fe3-O83	80.51(7)
		N60-Fe2-N51	81.84(10)	O93-Fe3-O83	96.62(8)
				O71-Fe3-O83	89.08(8)

Table S6 Selected bond lengths and angles [Å] for (**3**)

Bond lengths [Å]		Bond angles [°]					
Cu1-N30	2.022(3)	N30-Cu1-N21	80.86(11)	N60-Cu2-N41	168.70(10)	O91-Fe3-O75	167.19(8)
Cu1-N21	2.028(3)	N30-Cu1-N11	167.05(11)	N60-Cu2-N51	78.84(11)	O91-Fe3-O85	92.52(10)
Cu1-N11	2.030(2)	N21-Cu1-N11	94.02(10)	N41-Cu2-N51	96.51(11)	O75-Fe3-O85	97.36(10)
Cu1-N40	2.038(3)	N30-Cu1-N40	97.16(10)	N60-Cu2-N70	94.46(11)	O91-Fe3-O95	81.43(11)
Cu1-N20	2.285(3)	N21-Cu1-N40	165.96(11)	N41-Cu2-N70	92.13(10)	O75-Fe3-O95	90.39(12)
Cu1-N31	2.304(3)	N11-Cu1-N40	90.63(10)	N51-Cu2-N70	166.30(10)	O85-Fe3-O95	167.18(11)
Cu2-N60	2.031(3)	N30-Cu1-N20	91.75(11)	N60-Cu2-N50	91.61(10)	O91-Fe3-O81	95.13(10)
Cu2-N41	2.030(2)	N21-Cu1-N20	92.67(10)	N41-Cu2-N50	78.63(11)	O75-Fe3-O81	94.57(10)
Cu2-N51	2.146(3)	N11-Cu1-N20	76.54(11)	N51-Cu2-N50	96.79(10)	O85-Fe3-O81	80.30(8)
Cu2-N70	2.158(3)	N40-Cu1-N20	101.30(11)	N70-Cu2-N50	95.32(12)	O95-Fe3-O81	88.95(9)
Cu2-N50	2.159(3)	N30-Cu1-N31	94.74(10)	N60-Cu2-N61	93.73(10)	O91-Fe3-O71	90.55(10)
Cu2-N61	2.184(3)	N21-Cu1-N31	90.32(11)	N41-Cu2-N61	96.76(11)	O75-Fe3-O71	80.50(10)
Fe3-O91	1.995(3)	N11-Cu1-N31	97.18(11)	N51-Cu2-N61	92.30(12)	O85-Fe3-O71	95.03(9)
Fe3-O75	1.996(3)	N40-Cu1-N31	75.95(11)	N70-Cu2-N61	76.09(13)	O95-Fe3-O71	96.31(9)
Fe3-O85	2.003(2)	N20-Cu1-N31	173.21(9)	N50-Cu2-N61	170.20(11)	O81-Fe3-O71	172.78(11)
Fe3-O95	2.009(2)						
Fe3-O81	2.010(2)						
Fe3-O71	2.022(2)						

Table S7 Summary of Fe and Cu L-Edges and N and O K-edges for **1** and **2**.

Element and edge	Complex	Energy peak [eV]	Maximum of intensity [i]	Energy peak [eV]	Maximum of intensity [ii]
Fe L-edge	**1**	708.0, 710.0	10.47, 7.11	719.6(sh), 721.2, 723.2	1.94, 3.11, 2.01
Fe L-edge	**2**	708.1, 709.6	4.67, 7.62	721.3, 723.2(sh)	3.39, 2.04
Cu L-edge	**1**	931.2, 933.2, 934.8	3.00, 1.27, 1.32	951.0, 953.2, 954.3	1.45, 1.07, 1.14

For Fe and Cu [i] L_3 edge and [ii] L_2 edge.

Table S8 Magnetic parameters for (**1**)

No	Limit	g_{av}	$J_{Cu\text{-}Fe}$ [cm^{-1}]	$J_{Cu\text{-}Cu}$ [cm^{-1}]	C	zJ' [cm^{-1}]	R**
1	–	2.044	−3.383	0^*	0.05^*	−0.136	$5.93\cdot10^{-5}$
2	–	2.052	−3.372	-0.1^*	0*	−0.117	$8.22\cdot10^{-5}$
3	J' >= −0,5	2.053	−3.406	−0.5	0*	−0.119	$7.44\cdot10^{-5}$

* fixed parameter, ** $R = \sum(\chi'_{obs} - \chi'_{calc})^2 / \sum(\chi'_{obs})^2$

Thermal and spectroscopic properties

Thermal decomposition processes were not studied in details but for their final products powder diffractograms were registered.

Thermal decomposition of $[Cu_2(bpy)_4Fe(ox)_3]NO_3{\cdot}H_2O$ (**1**) studied by combined TGA–DTA techniques under an air atmosphere occurs in three steps. The compound is thermally stable and loss of mass starts at approximately 100°C. The first step related to dehydration (observed 1.58%, calc. 1.56%) is accomplished at 153°C. Subsequently, according to DTA two not clearly separated exothermic steps occurs (the second is strongly exothermic) with the continuous mass loss up to 360°C. During these stages bpy molecules as well as oxalate and nitrate anions are lost. Clemente-León et al. [2] established that oxalate anions can decompose in the range from 160 to 280°C. We did not study in detail of this decomposition, however, the mass residue of 20.6% indicates that the process results in mixture of CuO and Fe_3O_4 (theoretical value: 20.5%). Their presence was confirmed by powder XRD method registered for products of thermal decomposition. These data are consistent with results for copper complexes [3] for which Cu_2O was observed only for the decomposition processes carried out in nitrogen atmosphere, whereas processes studied in air resulted in CuO.

For (**2a**) we observe loss of mass starting at room temperature (*cf.* Experimental) proving that this compound is unstable. This step corresponds to loss of crystallization water molecules (experimental: 8.9%, theoretical value for $10H_2O$ is 11.2%) and is accomplished at 130ºC. The discrepancy between structural model and these data shows that at least two crystallization water are extremely unstable and are easily removed at RT. Subsequently, the second strongly exothermic step is observed characterized by the main mass loss (67.0%) which around 275ºC passes into the third and last step accomplished at *ca.* 390ºC with the mass residue 17.8%, whereas the theoretical value 14.9% corresponding to Fe_2O_3 confirmed by powder XRD method is lower than the experimental one.

Crystal degradation of (**3**) proceeds faster than for (**2**). Hence we concluded that the structure of (**3**) is even more unstable than (**2a**) and we can observe loss of mass starting at room temperature (*cf.* Experimental). This step corresponds to loss of crystallization water molecules (experimental: 10.1%, calc. 11.1%) and is accomplished at 120ºC. Subsequently, the second step is observed characterized by the main mass loss (55.6%) which around 330ºC passes into the third and last step accomplished at *ca.* 450ºC with the mass residue 16.0%. The details of this decomposition were not followed but products of thermal decomposition were studied by powder XRD and mixture of oxides (CuO + Fe_3O_4; theoretical: 14.5%) was detected.

(**1**) **IR**/cm^{-1}: 3431(br,s), 3108(w), 3062(m), 1706(w), 1665(vs), 1625(vs), 1493(m), 1474(m), 1445(m), 1422(w), 1383(m), 1338(w), 1274(w), 1251(w), 1221(vw), 1174(w), 1158(m), 1104(w), 1073(vw), 1057(vw), 1043(vw), 1029(m), 1012(m), 891(m), 827(vw), 811(sh,w), 772(s), 733(m), 660(w), 649(w), 635(w), 523(m), 450(m), 420(m) 410(m). **Raman**/cm^{-1}: 3070(vw), 2793(vw), 2646(vw), 2483(vw), 1595(s), 1560(s), 1478(vs), 1431(w), 1307(s), 1277(m), 1170(m), 1012(s), 763(w), 739(w), 647(m), 416(m).

(**2**) **IR**/cm^{-1}: 3425(br,s), 3075(m), 1709(w), 1666(vs), 1601(s), 1466(m), 1442(w), 1426(w), 1384(s), 1260(m), 1251(m), 1158(m), 1120(w), 1065(vw), 1043(vw), 1012(w), 900(m), 828(vw), 775(s), 734(m), 647(w), 526(w), 421(m). **Raman**/cm^{-1}: 1603(m), 1561(s), 1489(vs), 1323(s), 1273(s), 1174(m), 1025(m), 767(m), 662(m).

(**3**) **IR**/cm^{-1}: 3431(vs,br), 3103(m), 3073(m), 3028(m), 1709(s), 1670(vs), 1598(vs), 1575(w), 1553(w), 1492(w), 1472(s), 1442(vs), 1383(vs), 1368(m), 1313(m), 1263(m), 1249(m), 1228(w), 1176(m), 1158(m), 1102(m), 1072(m), 1062(w), 1043(vw), 1018(s), 906(w), 893(m), 828(w), 776(vs), 736(s), 651(m), 626(w), 584(vw), 527(m), 485(w), 417(m). **Raman**/cm^{-1}: 1603(m), 1560(s), 1489(vs), 1322(s), 1273(m), 1174(s), 1022(s), 766(vw), 660(m).

The IR spectra of all reported complexes present the characteristic absorptions of the 2,2'-bipyridine (bpy), oxalate, nitrate and water. For the coordinated bpy the bands in the range from 3108 to 3062 cm^{-1} correspond to C-H stretching, whereas bands in the range from 1516 to 1422 cm^{-1} are assigned to ν(C=C) and ν(C=N) as well as δ(C-H) vibrations in the aromatic ring [4,5,6,7]. In the studied complexes the presence of water molecules can be identified by the broad band at 3431–3425 cm^{-1} arising from stretching vibrations. In **1** the absorption bands occurring at 1706, 1665 (ν_a(CO)), 1383 (ν(CO)+ν(CC)), 1274, 1251 (ν(CO)+δ(OCO)), 811 (δ(OCO)+ν(Fe-O)) cm^{-1} correspond to the bidentate binding of oxalate, whereas bands at 1625 (ν_a(CO)) and 1338 ((ν(CO)+ν(CC)) cm^{-1} can be ascribed to bridging oxalate bound in bis(bidentate) mode [8,9]. Band at 523 cm^{-1} results from ring deformation+δ(OCO) vibrations of the coordinated oxalate ligand. In both, **2a** and **3**, bands positions are very similar to these observed for vibrations of bidentately coordinated non-bridging oxalate in the trimer. In all complexes non-coordinating nitrate anions show bands at *ca*. 1370 (ν_a(NO)) and *ca*. 830 ($\delta(NO_3)$) cm^{-1} [9]. In general, in **1** and **3** positions of the observed bands are usually very close to those in the corresponding chromium complexes [8].

In all complexes most of strong Raman active bands occurs in the range 1600–700 cm^{-1}, whereas vibrations in the range from 3200 to 2600 cm^{-1} and 600 to 100 cm^{-1} are usually much weaker. In all complexes vibrations in the range from 1603 to 1478 cm^{-1} correspond to C=C and C=N stretching, whereas bands at 1323, 1273 and 1170 cm^{-1} are due to in plane C-H deformations. Vibrations at *ca*. 1020 cm^{-1} are due to in plane ring and C-H bending, whereas band corresponding to in plane ring bending occurs at *ca*. 765 cm^{-1} [4,5,10,11].

*Crystal structure description of [Cu_2(bpy)$_4$Fe(ox)$_3$]NO_3·H_2O (**1**)*

This compound crystallizes in monoclinic C2/c space groups with iron atom positioned at the twofold axis and all remaining atoms found in the general positions. The structure contains [Cu_2(bpy)$_4$Fe(ox)$_3$]$^+$ cations but in the asymmetric unit half of the trimer consisting of [Cu(bpy)$_2$]$^{2+}$ moiety, iron atom, O21 oxalate anion and half of O31 one as well as partially occupied nitrate anion and water molecule are found. For outer non-coordinating oxygen atom from O31 oxalate two alternate equally populated (50/50) positions were found. The trimer is built of lateral [Cu(bpy)$_2$]$^{2+}$ units connected to the central [Fe(ox)$_3$]$^{3-}$ block *via* bridging O21 oxalates (Fig. S1).

The Fe(III) coordination sphere consists of six oxygen atoms coming from three oxalate anions with Fe-O bonds ranging from 1.9750(14) to 2.0383(14) Å (Table S2) being slightly shorter than Cr-O distances reported by Jurić et al. [8] (1.9454(16)–1.9900(16) Å). They are very similar to Fe-O bond lengths found in [Co(NH_3)$_5$(imH)][Fe(ox)$_3$]·6H_2O (1.986(2)–2.032(2) Å) and *fac*-[Co(hmH)$_3$)][Fe(ox)$_3$] ·5.5H_2O (1.988(3)–2.038(3) Å) [12] as well as *cis*-[Co(NH_3)$_4$(H_2O)$_2$][Fe(ox)$_3$]·2H_2O (1.9888(18)–2.0309(17) Å) [13]. Iron atom is found in slightly trigonally distorted octahedral environment with angles from 80.03(6) to 97.09(6)° and from 166.81(7) to 175.84(9)°. Much bigger distortions are found in copper environment with the valence angles falling into two very broad range from 80.17(6) to 178.88(6)° indicating also that the sphere is strongly distorted. The polyhedral analysis obtained with the SHAPE [14] software revealed the parameters sets S_{HP} = 29.62, S_{PPY} = 22.03, $\boldsymbol{S_{\mathrm{OC}}}$ **= 3.513**, S_{TPR} = 10.08, and S_{JPPY} = 24.65 for the 6-coordination regime, and S_{PP} = 28.34, $\boldsymbol{S_{\mathrm{VOC}}}$ **= 3.261**, $\boldsymbol{S_{\mathrm{TBPY}}}$ **= 3.513**, $\boldsymbol{S_{\mathrm{SPY}}}$ **= 2.874**, and S_{JTBPY} = 6.225 for 5-coordination regime. Such sets of shape measures does not allow for the strict definition of coordination environment, and we are forced to treat it either as a strongly distorted octahedron or polyhedron intermediate between trigonal bipyramid and square pyramid (τ_5 = 0.51 [15]). Among only three known Cu-Fe-oxalate complexes with bidentate-monodentate coordination mode 1D chains are formed by (NH_4)[Cu(en)$_2$Fe(ox)$_3$]·2dmso with oxalate coordinated bidentately to Fe(III) and monodentately to Cu(II) ion but *via* inner oxygen atom with Cu-O bonds being very long (2.769(3) – 2.869(3) Å) [16]. In [(Bpyph)Cu(H_2O)$_2$Fe(ox)$_3$]·6.5H_2O the bridging anion coupling four-coordinated copper and iron atoms is coordinated bisbidentately with both Cu-O bonds being comparable (2.424(6) and 2.432(6) Å) [17]. 3D network of {[Cu(en)$_2$][KFe(ox)$_3$]}$_n$ is the only compound with Cu(II) and Fe(III) coupled by mono-/bidentate coordinated oxalate with copper found in 4+2 coordination mode with two long Cu-O distances (2.567 and 2.801 Å) [18]. For 1D chains with bridging oxalates revealing mono(inner)/bidentate coordination the shortest intermetallic distances (Fe-Cu) were found from 4.263 to 4.358 Å, whereas for bisbidentately coordinated oxalate joining copper and iron into dimer they were longer (5.516 Å) [16,17].

In **1** both bpy molecules (N1 and N11) are flat within 0.033 and 0.119 Å, respectively, and they form an angle of 65.47(3)°. Hence, N11 molecule seems to be much more folded than N1 ligand. However, all pyridine rings forming N1 and N11 remains flat within 0.011 Å and the observed significant folding of N11 molecule is false and results from a twist between both six-membered rings being 14.11(11)°, whereas the angle in N1 ligand is 3.73(12)° and both pyridine rings are coplanar. Bridging O21 oxalate anion forms angles of 56.02(5) and 86.60(5)° for N1 and N11 molecules, respectively. The angles between oxalate anion in $[Fe(ox)_3]^{3-}$ moiety are 79.91(4) (O21/O21[-x+1, y, -z-1/2]) and 74.31(6)° for (O21/O31). Both oxalate anions are folded and the twist between two carboxylic groups is 15.55(44) and 12.00(41)° in bridging O21 and non bridging O31 anions, respectively. Similarly, these groups in the chromium analog are not coplanar and they are tilted by 14.05(12)° and 6.0(2)° in the bridging and terminal ligands.

*Crystal structure description of $[Cu(bpy)_3]_2[Fe(ox)_3]NO_3\cdot 10H_2O$ (**3**)*

The $[Cu(bpy)_3]_2[Fe(ox)_3]NO_3\cdot 10H_2O$ **3** complex crystallizes in the monoclinic $P2_1/c$ space group with all atoms in general positions and the whole molecule given by the formula in the asymmetric unit. The structure consists of two mononuclear $[Cu(bpy)_3]^{2+}$ cations, one $[Fe(ox)_3]^{3-}$ anion, one nitrate anion and ten crystallization water molecules.

Bpy ligands form torsion angles of 88.45(6) (N11/N21), 78.91(4) (N21/N31) and 89.45(6)° (N11/N31) for molecules surrounding Cu1 atom and 82.31(6) (N41/N51), 88.74(5) (N51/N61) and 86.02(6)° (N41/N61) for Cu2 atom. It indicates that these molecules are almost perpendicularly oriented to each other. All bpy ligands are flat within rms deviation of 0.081 Å, whereas deviations for pyridine rings are much smaller. It is due to small torsion angles formed by both pyridine rings forming bpy molecule reaching 9.41(18)° for N21 and N30 rings. The angles between oxalate anion in $[Fe(ox)_3]^{3-}$ moiety are 86.02(8) (O71/O81), 88.37(8) (O81/O91) and 81.04(5)° (O71/O91) and they are almost perpendicularly oriented. Both carboxylic groups from the same oxalate anion are almost ideally coplanar with angles 8.0(8), 2.5(7) and 2.5(7)° for O71, O81 and O91 oxalate anions, respectively.

In the case of both copper atoms six nitrogen atoms coming from three 2,2'-bipyridine ligands form a distorted octahedral environment. The valence angles of N-Cu1-N range from 75.95(11)–101.30(11)° and 165.96(11)–173.21(9)° (Table S6, Fig. S5) and from 76.09(13)–96.79(10)° and 166.30(10)–172.78(11)° for N-Cu2-N angles. The iron ion is bonded to six oxygen atoms coming from three oxalate ligands, which are arranged in a trigonally distorted octahedron with Fe–O bond lengths ranging from 1.995(3) to 2.022(2) Å and the O-Fe-O bond angles from 80.30(8)° to 97.36(10)° and 167.43(7)–172.77(11)°. Among ten water molecules O2 is the only molecule positioned in voids of hydrophobic copper sublattice playing crucial role in the crystal network formation. This molecule transmits interactions between two iron layers forming two strong hydrogen bonds: O2-H2A…O92[x, ½-y, -½+z] and O2-H2B…O76[x, y, z]. Mutually, iron sublattice penetrating space between copper columns participates also in interactions transmitted between copper pillars. Additionally, crystal network interactions are completed by C-H…π interactions and N-O…π interactions.

Comparison of bond lengths in coordination spheres of Cu(II) and Fe(III).

In the reported compounds Fe-O bonds are similar and range from 1.9750(14) to 2.0383(14) Å, from 1.996(2) to 2.011(2) Å, from 1.996(3) to 2.022(2) Å for (**1**), (**2**) and (**3**), respectively. These values are comparable to bond lengths reported for $[Co(NH_3)_5(imH)][Fe(ox)_3]\cdot6H_2O$ (1.986(2)–2.032(2) Å) and *fac*-$[Co(hmH)_3)][Fe(ox)_3]\cdot5.5H_2O$ (1.988(3) to 2.038(3) Å) [12], *cis*-$[Co(NH_3)_4(H_2O)_2][Fe(ox)_3]\cdot2H_2O$ (1.9888(18)–2.0309(17) Å) [13], in 3D network of $[Fe(bpy)_3][NaFe(ox)_3]$ (1.986(2)–2.002(2) Å) [19], in 1D chains formed by $[(Bpyph)Cu(H_2O)_2Fe(ox)_3]\cdot6.5H_2O$ (Bpyph = 1,4-bis(4'-pyridyl-1'-pyridinio)phthalazine cation, 1.972(6)–2.027(5) Å) [17] and in 1D chains of $(NH_4)[Cu(en)_2Fe(ox)_3]\cdot2dmso$ (1.998(4)–2.020(3)Å) despite in the latter case bridging oxalate is found in mono/bidentate coordination mode [16]. In $(Bpyph)_2\{M^{II}(H_2O)_2[Fe(ox)_3]_2\}\cdot12.5H_2O$ trimers (M^{II} = Mn, Co; 1.976(2)–2.064(3) Å) [20] broad range of Fe-O bond lengths is observed with the longest bonds corresponding to the bridging oxalate anion. In (**2**) Fe-N bonds range from 1.970(3) to 1.982(3) Å. They are similar to values found by Armentano et al. [21] (1.968(5)–1.989(6) Å), Decurtins et al. [19] (1.971(2)–1.977(2) Å). For $[Fe^{II}(bpy)_3]_2[Fe(ox)_3]\cdot12.25H_2O$ Wang et al. [22] found Fe-N bonds ranging from 1.979(5) to 1.988(5) Å. Contrary, for two compounds *i.e.* $(AsPh_4)[Fe(bpy)(ox)_2]\cdot H_2O$ and $(AsPh_4)[Fe(phen)(ox)_2]\cdot H_2O$, Fe^{III}-N bonds are very long ranging from 2.140(3) to 2.171(3) Å [21]. Hence, analysis of Fe-N bonds is easy and reliable method of discrimination between Fe(II) and Fe(III) ions. Copper sphere is much more distorted in the reported compounds with Cu-N bonds being 1.9695(16)–2.1137(16) Å and 2.022(3)–2.304(3) Å for (**1**) and (**3**), respectively. It is clear that there are three principal Cu-N bond ranges: the shortest Cu-N distances are close to 1.98–2.07 Å, 2.15–2.18 Å and 2.28–2.31 Å. Cu-N bonds ranged from 1.968(2) to 2.037(2) and from 2.107(2) to 2.179(2) in $[Cu(bpy)_2(CH_3COO)][Cu(bpy)_2(Cr(ox)_3)]\cdot10.5H_2O$ with five-coordinated copper ions [23]. In $[(Bpyph)Cu(H_2O)_2Fe(ox)_3]\cdot6.5H_2O$ with four-coordinated Cu(II) ions these distances are very short (1.927(5) and 1.938(6) Å) [15]. In the structure reported by Vallejo et al. [24] Cu-N distances range from 1.967(4) to 1.978(4) Å, whereas for dimers reported by Lescouëzec et al. [25] they fall in the range from 1.922(3) to 2.017(3) Å. Much severe differences were observed for Cu-O bonds. In the structure reported by Chygorin et al. [16] oxalate coordinates monodentately to Cu(II) ion *via* inner oxygen atom coordinating also to iron(III) and Cu-O bonds are extremely long ranging from 2.769(3) to 2.869(3) Å, whereas for four-coordinated copper(II) ions in $[(Bpyph)Cu(H_2O)_2Fe(ox)_3]\cdot6.5H_2O$ these distances are much shorter but still they remain long

(2.432(6) and 2.424(6) Å) [17]. In $\{[Cr(bpy)(ox)_2]_2Cu_2(bpy)_2(ox)\}\cdot 6H_2O$ with Cr-Cu-Cu-Cr tetramers these distances are short for a central oxalate exposing bisbidentate coordination (1.968(4) and 1.969(4) Å), whereas oxalate showing monodentate binding was found at 2.383(4) Å [24]. In dimers with oxalate forming a bridge due to mono/bidentate coordination Cu-O bonds are long (2.253(2) and 2.325(4) Å) [25], whereas in $[Cu(bpy)_2(CH_3COO)][Cu(bpy)_2Cr(ox)_3]\cdot 10.5H_2O$ this bond is significantly shorter (2.078(2) Å) [23].

References

---

[1] M. A. Spackman, J. J. McKinnon, *CrystEngComm*, 2002, **4**, 378–392.

[2] M. Clemente-León, E. Coronado, M. C. Giménez-López, F. M. Romero, S. Asthana, C. Desplanches, J.-F. Létard, *Dalton Trans.*, 2009, 8087–8095.

[3] R. Szczęsny, T. M. Muzioł, D. H. Gregory, E. Szłyk, *Chem. Pap.*, 2015, **69**, 569–579.

[4] G. Socrates, *Infrared and Raman Characteristic Group Frequencies*, Tables and Charts, Third Ed., Wiley, Chichester, 2004, pp 168–171.

[5] E. Castelluci, L. Angeloni, N. Neto, G. Sbrana, *Chem. Phys.*, 1979, **43**, 365–373.

[6] J. S. Strukl, J. L. Walter, *Spectrochim. Acta,* 1971, **27A**, 209–221.

[7] J. R. Ferraro, W. R. Walker, *Inorg. Chem.*, 1965, **4,** 1382–1386.

[8] M. Jurić, P. Planinić, N. Brničević, D. Milić, D. Matković-Čalogović, D. Pajić, K. Zadro, *Eur. J. Inorg. Chem.,* 2006, 2701–2710.

[9] K. Nakamoto, *Infrared and Raman Spectra of Inorganic and Coordination Compounds*, pt B, Sixth Ed., Wiley, Hoboken, New Jersey, 2009, Vol. A., pp 180–184, Vol. B, pp 79–82.

[10] T. P. Gerasimova, S. A. Katsyuba, *Dalton Trans.*, 2013, **42**, 1787–1797.

[11] B. D. Alexander, T. J. Dines, R. W. Longhurst, *Chem. Phys.*, 2008, **352**, 19–27.

[12] T. M. Muzioł, G. Wrzeszcz, Ł. Chrząszcz, *Polyhedron*, 2011, **30**, 169–177.

[13] T. M. Muzioł, G. Wrzeszcz, *Polyhedron*, 2016, **109**, 138–146.

[14] M. Llunel, D. Casanova, J. Cirera, J. M. Bofill, P. Alemany, S. Alvarez, M. Pinsky, D. Avnir, *SHAPE v. 2.1. Program for the Calculations of Continuous Shape Measures of Polygonal and Polyhedral Molecular Fragments*, University of Barcelona, Spain, 2013.

[15] A. W. Addison, T. N. Rao, J. Reedijk, J. van Rijn and G. C. Verschoor, *J. Chem. Soc., Dalton Trans.*, 1984, 1349.

[16] E. N. Chygorin, V. G. Makhankova, V. N. Kokozay, V. V. Dyakonenko, O. V. Shishkin, J. Jezierska, *Inorg. Chem. Commun.*, 2010, **13**, 1509–1511.

[17] Y.-Q. Sun, J. Zhang, G.-Y. Yang, *Dalton Trans.*, 2003, 3634–3638.

[18] G.-M. Yang, H.-Z. Kou, D.-Z. Liao, Z.-H. Jiang, S.-P. Yan, G.-L. Wang, X.-K. Yao, H.-G. Wang, *Huaxue Xuebao (Chin.) (Acta Chim. Sinica)*, 1999, **57**, 998.

[19] S. Decurtins, H. W. Schmalle, P. Schneuwly, J. Ensling, P. Gütlich, *J. Am. Chem. Soc.*, 1994, **116**, 9521–9528.

[20] Y.-Q. Sun, J. Zhang, G.-Y. Yang, *Dalton Trans.*, 2006, 1685–1690.

[21] D. Armentano, G. De Munno, F. Lloret, M. Julve, *CrystEngComm*, 2005, **7**, 57–66.

[22] X. Wang, Y. Xu, X. Song, L. Li, D. Liao, Z. Jiang, S. Yan, *J. Chem. Crystallogr.*, 2007, **37**, 651–654.

[23] O. Costisor, K. Mereiter, M. Julve, F. Lloret, Y. Journaux, W. Linert, M. Andruh, *Inorg. Chim.*

Acta, 2001, **324**, 352–358.

[24] J. Vallejo, I. Castro, M. Déniz, C. Ruiz-Pérez, F. Lloret, M. Julve, R. Ruiz-García, J. Cano, *Polyhedron*, 2013, **52**, 1246–1255.

[25] R. Lescouëzec, G. Marinescu, J. Vaissermann, F. Lloret, J. Faus, M. Andruh, M. Julve, *Inorg. Chim. Acta*, 2003, **350**, 131–142.